A Co-Delivery Strategy of Abemaciclib Combined with Vitamin E Succinate Based on Hyaluronic Acid Modified Calcium Phosphate to Enhance the Anti-Cancer Effect

Yuanyuan Liu
Sichuan University
Na Gan
Sichuan University
Shuangshuang Zhang
Sichuan University
Qiaomei Sun
Sichuan University
Xin Wei
Sichuan University
Xiuyun Ren
Sichuan University
Xi Xiang
Sichuan University
Hui Li (lihuilab@sina.com)
Sichuan University

Research Article

Keywords: Calcium phosphate, Hyaluronic acid, Drug co-delivery, Abemaciclib

Posted Date: July 20th, 2021

DOI: https://doi.org/10.21203/rs.3.rs-729230/v1

Abstract

Combination therapy including anticancer drugs usually induces synergistic effects, especially in combination with natural compounds as a chemical sensitizer. Nano-based drug delivery technology is also effective in solving the toxicity of single drugs at high doses. In this study, we established a co-delivery strategy for abemaciclib (ABE) combined with vitamin E succinate (VES) based on HA-modified calcium phosphate (CaP) nanomaterials to enhance anti-cancer effect. The nano-sized HA/CaP particles (90 nm) have a hollow structure. Surprisingly, after modification with HA, HA/CaP has more pH sensitivity. CaP released 30% ABE and 91% VES at pH 7.4, whereas HA/CaP vsreleased 14% ABE and 32% VES at the same pH. Cell experiments showed that HA/CaP/ABE-VES had stronger cell inhibitory effect on MCF-7 compared with CaP/ABE-VES. This inorganic/organic composite for the co-delivery of ABE and VES has obvious tumor inhibition effect, and is ideal for anti-tumor drug delivery.

1. Introduction

CDK 4/6 inhibitor abemaciclib (ABE) plays a central role in tumor formation, and has become an important molecular target drug for the clinical treatment of breast cancer[1]. However, clinical data shows that the objective remission rate of ABE is only 19.7%[2]. The anti-tumor effect of ABE still needs to be improved by other strategies, such as combination therapy. A variety of cyclin D-related signaling pathways (like estrogen epidermal growth factor receptor, phosphoinositide 3-kinase and NF-κB) have great potential in combination with ABE [3, 4].The natural derivative of vitamin E, vitamin E succinate (VES), has attracted people's attention because of its synergistic anticancer activity[5, 6]. VES has been reported to induce apoptosis of cancer cells by inhibiting the NF-κB[7, 8]. The combination of ABE and VES has synergistic potential in the treatment of breast cancer.

Moreover, multimodal cancer therapy, which combines chemotherapy and multifunctional nanomaterials, has remarkably improved the efficacy of cancer therapy and may provide a better solution to overcome the poor efficacy of single chemotherapeutic agents[9, 10]. Calcium phosphate (CaP)-based nanocarrier materials pH responsiveness as they can decompose under acidic conditions; thus, they have a wide range of applications in the field of biological medicine, including transfection, gene silencing, drug delivery, and biological imaging[11, 12]. The incorporation of Hyaluronic acid (HA) can make nanoparticles (NPs) specifically bind to the CD44 receptor on the surface of CD44-overexpressed tumor cell. The HA layer also could improve the stability of the nanocomposite, which significantly enhance cellular uptake[13, 14]. Based on this foundation, Xiong and colleagues reported HA-modified NPs with high drug loading efficiency and pH-responsive drug release[15]. Min and colleagues prepared 3, 4-dihydroxy-L-phenylalanine-coupled HA-stabilized CaP NP for the targeted delivery of siRNA to tumor sites[16]. This gene delivery platform shows great potential for siRNA delivery and targeted cancer therapy. But most of the researches on CaP and HA are focus on gene drug delivery and stagnate in single-drug delivery[17, 18]. As a widely studied drug carrier, CaP and HA still have potential for further application in drug co-delivery. More effective strategies for the treatment breast cancer need to be

developed to solve the poor effect of ABE and improve the benefits of anticancer therapies without attendant toxicity.

We expect that the HA/CaP system can load two drugs at the same time, which could fully use dual drug synergy and nano-carrier drug delivery system. With this idea in mind, this study designed a HA-coated and CaP-based drug delivery system for the controlled release of ABE and VES, to achieve the effective controlled drug release of nano-carrier and a synergistic anti-cancer effect for breast cancer.

2. Materials And Method

2.1 Materials

Abemaciclib (FW = 506.59, purity ≥ 98%) was purchased from Shanghai Topbiochem Technology Co. Ltd. (Shanghai, China),vitamin E succinate (FW = 530.78, purity ≥ 98%) and sodium hyaluronate (FW: 100–200 kDa) were attained from Heowns (Tianjin, China). NaOH, phosphate buffer solution (PBS), disodium hydrogen phosphate, calcium chloride, hydrochloric acid, methanol, acetic acid, and ammonium acetate were obtained from Ke-Long Chemical Reagent Factory (Chengdu, China). Purified water was used throughout the experiment. All of the reagents and chemicals used in this study were of analytical or chromatographic grade and used without further purification.

2.2 Preparation of CaP and HA/CaP NPs

Cetyltrimethylammonium bromide (CTAB) was dissolved in 50 mL of water to a concentration of 1 mM. The solution was stirred for 10 min at 500 rpm (room temperature) to obtain the CTAB micelle. The mineralized micelles were prepared by the classical chemical precipitation method according to previous literature reports [19, 20]. The details are as follows: Na_2HPO_4 (2 mL, 60 mM) was added drop dropwise into the solution containing CTAB micelles at 500 rpm and 45°C After 0.5 h, 2 mL of 100 mM $CaCl_2$ was added into a 50 mL solution containing 1.2 mM Na_2HPO_4 and 1 mM CTAB under magnetic stirring (pH = 10.0, pH was adjusted by 0.1 M ammonia solution) for 1 h. The temperature was kept at 45°C by water bath. The suspension was aged at room temperature for 3 h, and the precipitate was washed with purified water three times. CaP product was obtained after 24 h of freeze-drying. The "one-pot " method was used to prepare HA/CaP NPs. Sodium hyaluronate solution (2%, m/v) was added dropwise to the CaP nanosphere suspension. The suspension was aged at room temperature for 3 h. The precipitate was washed three times with purified water and freeze-dried for 24 h to obtain the HA/CaP product.

2.3 Drug encapsulation experiment

ABE and VES were dissolved in ethanol then to CTAB micellar solution to obtain CaP/ABE-VES and HA/CAP/ABE-VES. The quantification of dual-drug was determined by high performance liquid chromatography (Agilent 1200, USA). Before that, we tested the effect of blank carrier on drug absorption using ultraviolet-visible spectrophotometry (Shimadzu, Japan). The detailed measurement of drug content is as follows: NPs were dissolved in 0.1 M hydrochloric acid, dilute with methanol, and

ultrasonicated for 10 min to destroy the structure of CaP/ABE-VES and HA/CaP/ABE-VES. After cooling to room temperature, the NPs were filtered with 0.22 μm micropores. Retention time and peak area were recorded, and the contents of ABE and VES were calculated at 296 and 284 nm according to the regression equation. The formulas for calculating the drug loading rate (DL) and encapsulation efficiency (EE) are as follows:

$$\mathrm{DL}\% = \frac{Weight\ of\ drug\ in\ nanoparticles}{Total\ weight\ of\ drug\ loaded\ nanoparticles} \times 100\% \quad (1)$$

$$\mathrm{EE}\% = \frac{Weight\ of\ drug\ in\ nanoparticles}{Weight\ of\ feeding\ drug} \times 100\% \quad (2)$$

2.4 Characterization of CaP and HA/CaP NPs

Nicolet 6700 Fourier infrared spectrometer (Thermo Fisher Technology Co., Ltd., USA) was used to test the prepared CaP, HA/CaP, CaP/ABE-VES, HA/CaP/ABE-VES, physical mixture (PM) and active pharmaceutical ingredient (API) by KBr tablet method. The samples to be tested consist of 100 mg KBr and 1 mg sample. The sample mixture was pressed into a sheet of about 1 mm, the wavenumber was set between 4000 and 400 cm^{-1}, the resolution is 4 cm^{-1}, and the number of scans was 64 times.

The degrees of crystallinity were measured by X'Pert PRO diffractometer (PANalytical, Netherlands). The test conditions were as follows: Cu Kα radiation, tube voltage was 40 kV, tube current was 40 mA, 2θ range was set between 5 and 50°, anti-scatter slit was 1/4°, scattering slit was 1/8°, step size was 0.01313°(2θ), and counting time was 30 ms/step.

A JSM-7500F scanning electron microscope (Olympus, Japan) and a JEM-2100 Plus transmission electron microscope (JEOL, Japan) were used to observe the morphology of the prepared CaP and HA/CaP NPs. The NPs for TEM characterization were dispersed in the aqueous solution, dropped onto a copper mesh covered with a carbon film, air-dried, and placed in a detector for observation. The INCA X-Max50 energy spectrometer equipped with SEM system was used for semi-quantitative elemental analysis of CaP, HA/CaP, CaP/ABE-VES and HA/CaP/ABE-VES.

The prepared CaP and HA/CaP NPs were tested for hydrodynamic diameter and zeta potential using ZEN3690 nanoparticle size potential analyzer (Malvern, UK) at 25°C. The sample was dispersed in purified water at a concentration of 0.1 mg/mL.

An automatic surface area and porosity analyzer (3H-2000PS2, Beishiide) was used to measure the N_2 adsorption-desorption isotherm at 293.15 K. The Brunauer-Emmett-Teller (BET) method was used to calculate the specific surface area at a relative pressure ranging from 0.05 to 0.95. Pore volume and pore size distribution were obtained from the desorption curve of the isotherm using the Barrett-Joyner-Halanda (BJH) method.

Thermal analysis was performed on the TG 209F1 Iris thermogravimetric analyzer (NETZSCH, Germany) with a heating rate of 10°C/min, a temperature setting range of 30–600°C, and a nitrogen flow of 60 mL/min.

2.5 In vitro drug release

Drug release performance is one of the criteria whether a drug carrier can be practicallt used[21]. The tumor microenvironment is weakly acidic, at a pH range within 4.5–6.5, whereas the pH of the blood is about 7.4. We uses PBS with different pH values (pH = 4.5, 7.4) to simulate drug release in tumor and normal tissues for 8 h and calculated the cumulative release rates of the two drugs.

PBS containing 0.2 mol/L KH_2PO_4 with pH = 4.5 was prepared, and PBS with pH = 7.4 was obtained by adjusting the pH with 0.2 M NaOH. In order to increase the dissolution of poorly soluble drugs, 0.1% Tween 80 was added to the PBS to obtain the required dissolution medium. The drug dissolution experiment was carried out in a constant temperature shaker at 37°C and 200 rpm. Samples (1 mL) were pipetted at 5 min, 10 min, 1 h, 4 h, and 8 h for test and 1 mL of fresh dissolution medium at the same temperature was added to maintain the total volume of the release medium unchanged. The taken-out solution was filtered through a 0.22 μm microporous membrane. Cumulative release rate *R (%)* was calculated. Each experiment was done in parallel three times, and take the average value.

$$R(\%) = \frac{C_n \times V_0 + V_i \sum_{i=1}^{n-1} C_i}{m} \times 100\% \qquad (3)$$

where: C_n is the drug concentration of the sample to be tested for the n-th time (mg/mL); C_i is the drug concentration of the dissolution medium at the i-th sampling; V_0 is the total volume of the release medium (mL); V_i is the sampling volume; m is the total mass (mg) of the drug contained in the sample.

2.6 In vitro cytotoxicity

Cell counting kit 8 (CCK8) assay was used to measure cell viability. Briefly, 293T and MCF-7 cells were added in the 96-well plates at 37°C with 5% CO_2 for 24h. Free ABE and VES (100 μL) in Dulbecco's modified Eagle medium (DMEM) and cell culture medium containing gradient concentrations of carriers either with or without drug (6.25–200 μg/mL) were added to these cells after removing the old medium. After 48 h, 10 μL of CCK8 solution was added to each well, incubated for 2 h, and placed in a microplate reader (SoftMax Pro 7.1) to measure the optical density value at 450 nm. Cell inhibition rate was calculated, and IBM SPSS Statistics 24 software was used to calculate the half maximal inhibitory concentration (IC_{50}). The formula for calculating cell inhibition rate is as follows:

$$\text{Cell inhibition rate}(\%) = \left(1 - \frac{\text{Experimental group} - \text{Control group}}{\text{Negative control group} - \text{Control group}}\right) \times 100\% \qquad (4)$$

3. Results And Discussion

3.1 Preparation of blank and drug-loaded NPs

The UV spectra of ABE, VES, CaP and HA are shown in Fig. 1. CaP and HA/CaP have no UV absorption in the range of 250–400 nm, indicating that blank carriers will not interfere with the content determination of ABE and VES. The quantitative results showed that the drug loading rates and encapsulation rate of ABE in the CaP/ABE-VES system were 4.02% and 20.11%, respectively, whereas those of VES were 14% and 69.54%, respectively. The drug loading rate and encapsulation rate of ABE in the HA/CaP/ABE-VES system were 3.65% and 18.24%, respectively, whereas those of VES were 16% and 78.79%, respectively. The drug-loading effects of both systems were better on VES than ABE. This outcome may be helpful because VES is harmless to normal cells as a chemical sensitizer; thus, it could reduce the dosage of ABE and increase anti-cancer activity. This conclusion is verified in the results of subsequent cell viability experiments.

3.2 Shape, particle size, and zeta potential

CTAB micelles further formed to to CaP nanospheres with multivesicular structure and a particle size of about 80 nm under the deposition and mineralization of phosphate and calcium salt (Fig. 2A). The particle size of HA/CaP increased to 90 nm because of the presence of a 10 nm HA shell (Fig. 2B). The SEM results show that CaP has a nano-sized spherical structure and uniform overall morphology. HA/CaP is denser under SEM. This is because the negative charge carried by HA neutralizes the positive charge on the surface of CaP, which weakens the repulsive force against agglomeration on the surface of NPs. Particle size distribution curve (Figs. 2C and 2D) shows that the average hydrodynamic diameter of CaP and HA/CaP measured by dynamic light scattering (DLS) is about 100 nm and 110 nm. The particle size of the sample measured by the electron microscope is smaller than the value measured by the DLS due to the shrinkage and the reduction during the external force of air drying. As shown in Fig. 2D, zeta potential measurement shows that the surface charge of CaP is about 9.4 ± 0.80 mV, this indicates the presence of Ca^{2+} on CaP surface. The surface potential of HA/CaP decreased to -4.3 ± 0.25 mV, indicating that Ca^{2+} on the surface of CaP changed into carboxyl anion after HA covered on it, which confirmed that HA was successfully coated on the surface of CaP. Above results show that CaP with a spherical hollow structure was successfully prepared and HA coats on the surface of CaP under electrostatic interaction.

3.3 Infrared analysis

Figures 3A and 3B shows the infrared spectra of blank and drug-loaded CaP and HA/CaP. The absorption at 1036 cm^{-1} is attributed to the stretching vibration of the P-O bond. The characteristic absorption at 604 cm^{-1} and 566 cm^{-1} is caused by the bending vibration of O-P-O. This indicates that CaP with a hydroxyapatite structure was successfully prepared[22]. The absorption peaks of HA at 3423 cm^{-1}, 2923 cm^{-1}, and 1044 cm^{-1} correspond to the stretching vibrations of its carboxyl, methylene and C-O groups, respectively. Compared with CaP, the absorption of HA/CaP at 2923 cm^{-1} is enhanced, as a result of the presence of increased methylene groups in the HA molecule. Infrared spectroscopy analysis also

confirmed the presence of ABE and VES in drug carriers. The absorption band in the wavenumber range of 1400–1600 cm^{-1} is caused by the benzene ring vibration of ABE, and the double peaks in the spectrum of PM at 1715 cm-1 and 1753 cm-1 correspond to the carbonyl absorption of ester and carboxyl groups in VES. Those peaks appears in PM, but disappears in CaP/ABE-VES and HA/CaP/ABE-VES, this phenomenon may be due to the in-situ loading effect of the nanomaterials on the drug, which makes the drug molecules doped inside the material and causes peaks to weaken or disappear. The infrared results confirm that the prepared CaP is a calcium-deficient hydroxyapatite, and the drugs are encapsulated in the nanomaterials because of the in-situ drug-loading effect.

3.4 Crystallinity and element analysis

All of synthesized products showed hydroxyapatite-like characteristics in X-ray diffraction (XRD) analysis. CaP has two characteristic peaks at 26° and 32°. It can be indexed as a calcium-deficient hydroxyapatite structure with poor crystallinity[23]. The poor crystallinity is attributed to the low reaction temperature (40°C), which is consistent with reported literature, that is, CaP particles synthesized at low temperatures often show low crystallinity, high solubility and large specific surface area[24]. This result is conducive because a study on the resorption of biomaterials for hard tissue treatment showed that low-crystalline CaP is more degradable than CaP synthesized by sintering or other methods[25]. Therefore, the synthesized calcium-deficient CaP nanomaterials may have better biocompatibility. Figures 3C and 3D indicates that the drug is not simply mixed after being loaded in situ by CaP and HA/CaP. This result was consistent with the infrared result. The characteristic diffraction peak of HA/CaP/ABE-VES at 26° is weaker than that of blank HA/CaP. This may be due to the hydrogen bond between HA and the two drugs. The hydrogen bonding between the drug and the carrier resulted in lower crystallinity[26]. Energy-dispersive X-ray spectroscopy analysis showed a 1.5 Ca/P ratio, which further indicates that the synthesized CaP is a kind of calcium-deficient hydroxyapatite with poor crystallinity[27]. The C, O, and F elements in HA/CaP/ABE-VES also increased, indicating that the incorporation of HA can increase the drug loading of nanomaterials (**Fig. S1**).

3.5 Specific surface area and pore size distribution

As shown in Figs. 3E and 3F, the surface area of the CaP nanospheres is 123.90 $m^2 g^{-1}$. CaP has a large specific surface area, which is beneficial to the adsorption and loading of small molecule drugs. The surface area of CaP decreased to 89.94 $m^2 g^{-1}$ after coating with HA, because some mesoporous channels were covered by HA, resulting in a decrease in specific surface area. This phenomenon has also been found in previous literature[28]. N_2 adsorption curve of CaP shows that it has an obvious mesoporous structure. Figure 3 shows that the pore size of CaP is approximately 31.78 nm. The pore size distribution of HA/CaP is more uniform. After the addition of HA, pore size and pore volume were reduced to 29.74 nm and 0.67 $cm^3 g^{-1}$, respectively,. This decrease may be because the incorporation of negatively charged HA makes the internal electrostatic force of mesoporous HA/CaP stronger, which results in a more compact structure. This result is consistent with the conclusion of SEM.

3.6 Thermogravimetric (TG) analysis

The thermal decomposition is shown in Fig. 4. The endothermic peak of ABE and VES appeared at 360°C and 306°C, respectively. In the range of 150–350°C, CaP shows a weight loss of 4.04% at 333°C, which is attributed to the decomposition of the CaP framework[29]. The derivative thermogravimetric (DTG) curve of CaP/ABE-VES shows that the endothermic peak at 150–350°C becomes larger and the weight loss is 11.02%. This result is because of the overlap in the endothermic peaks of VES and CaP in this temperature range. A weight loss of 2.26% appears at 406°C, which corresponds to the endothermic peak of ABE in CaP/ABE-VES. The curve of HA/CaP/ABE-VES shows that the mass loss in this range is 26.59%, which is higher than that of CaP/ABE-VES. These results indicate that the HA/CaP system has a higher drug loading capacity for VES than a single CaP system. The higher drug loading capacity of HA/CaP may be due to the COO- group contained in the outer HA, which can provide more binding sites and space for drug molecules. The drug molecule may bind to the C site of CaP through electrostatic force, or be incorporated into the amorphous region of CaP through the Ca bridge action of the P site[30]. The thermal decomposition temperature of loaded drugs is higher compared with free drugs. This result also shows that the prepared HA/CaP can improve the thermal stability of the loaded drug.

3.7 pH Sensitivity of CaP and HA/CaP NPs

The drug release kinetics of CaP may be controlled by acid-assisted dissolution [31]. In pH 7.4, about 30% of ABE was released from CaP/ABE-VES after 8 h, which is higher than the 16% release of a single drug. When the pH dropped to 4.5, the cumulative release of ABE from CaP/ABE-VES can increased to 98% after 8 h but the release of a single drug at pH 4.5 is only 60%. In general, CaP makes the release of ABE more complete at pH 4.5. About 90% of VES was released from CaP/ABE-VES in 8 h at pH 7.4, which is similar to the 80% release of a single drug. The increased release of VES at pH 7.4 is due to the fact that VES is a weakly acidic molecule, and alkaline condition can increase its solubility. When the pH dropped to 4.5, the cumulative release of VES from CaP/ABE-VES can reach 100% after 8 h, whereas only 18% of the single drug was released. Therefore, the pH sensitivity of CaP as a carrier is weak for the controlled release of VES, that is, drug release can be achieved regardless of pH (4.5 or 7.4). Compared with the CaP system, the HA/CaP system released less drugs under acidic conditions. Whereas HA/CaP released only 14% ABE and 32% VES at pH 7.4. This may be because the covering effect of the HA layer prevents the dissolution of the drug. It is surprising that the incorporation of the HA layer greatly reduced the release of ABE and VES at pH 7.4, that is, the HA/CaP/ABE-VES system has stronger pH responsiveness, can release both drugs at pH 4.5, but few released at pH 7.4. Such release characteristics may weaken the damage of the drug to normal human cells, while killing cancer cells.

3.8 In vitro cytotoxicity evaluation of CaP and HA/CaP nanomaterials

The toxicity of the nanocarriers to normal cells and cancer cells were significantly different (Fig. 6**(a)** and Fig. 6**(b)**). When the concentration of CaP and HA/CaP was greater than 50 μg/mL, the proliferation of MCF-7 was significantly inhibited. Even the concentration reached up to 200 μg/mL, the viability of 293T

cells was above 90% ($p < 0.001$). The results indicate that the prepared nanomaterials are more damaging to cancer cells, other than normal cells, this is because the increase in calcium ions in the acidic environment of the tumor results in cell death[32].

VES can inhibit the proliferation of a variety of cancer cell, including human neuroblastoma cells, prostate cancer cells, promyelocytic cells, and breast cancer cells but is non-toxic to normal cell lines[33]. The experimental results on the cytotoxicity of VES are consistent with these reports. In vitro cytotoxicity of VES on 293T and MCF-7 cells are shown in Fig. 6**(c)**. VES had no significant inhibitory effect on 293T cells at concentrations up to 200 μM. By contrast, MCF-7 cells was significantly inhibited at the VES concentration of 50 μM ($p < 0.05$).

The stronger inhibitory effect on MCF-7 may be due to the synergistic effect of the two drugs, which strengthened the anti-tumor effect (Fig. 7**(b)** and Fig. 7**(d)**). HA/CaP still retained the Ca^{2+}-mediated inhibition of cancer cell proliferation after the dissolution of CaP in the acidic environment of the tumor. On this basis, the surface coating of the HA layer might have further increased the endocytosis of HA/CaP at low concentration, to enhance the inhibition of tumor cells at low concentration and consequently reduce the damage to normal cells. The results indicated that the prepared HA/CaP/ABE-VES utilizes unique pH responsiveness to effectively control the release of the drugs. This result is consistent with the results of the in vitro release experiment described in the previous section. The incorporation of HA endows HA/CaP/ABE-VES with stronger cytostatic effect on MCF-7 compared with that without HA.

3.9 Synergistic effect

Table 1
Evaluation of combined index (CI) at IC_{50}(ABE) in CaP/ABE-VES and HA/CaP/ABE-VES system

Drug/Combo(μM)	ABE	VES	PM-CaP	Co-CaP	PM-HA	co-HA
$IC_{50(ABE)}$	8.106	/	9.811	4.322	9.002	3.673
$IC_{50(VES)}$	/	484.767	34.339	15.127	40.509	16.529
CI value	/		1.337	0.327	0.983	0.188

Combination index (CI) value was calculated using CompuSyn software. The curve of log (CI) value and drug effect level (Fa) can clearly show the characteristics and extent of drug interaction[34]. Log (CI) values of > 0, 0, and < 0 mean antagonism, superimposition, and synergy, respectively[35]. In this study, the CI values of (PM) and CaP/ABE-VES on MCF-7 cell were compared. The CI value of HA/CaP/ABE-VES is 0.188, which has a stronger synergy (++++) and is lower than that of CaP/ABE-VES (CI = 0.327). In the CaP/ABE-VES and HA/CaP/ABE-VES group, all the log (CI) values in each corresponding Fa value are lower than log (CI) = 0. The mixed cocktails almost exceed log (CI) = 0. These results indicate that the synergistic effect of HA/CaP/ABE-VES and CaP/ABE-VES on MCF-7 cells is more remarkable than that of

the cocktail mixture. In addition, HA/CaP/ABE-VES presents a more remarkable synergistic anti-tumor effect than CaP/ABE-VES because of HA modification.

4. Conclusion

In this study, a pH-sensitive dual-drug-loaded nanocomposite material was prepared. HA/CaP/ABE-VES can effectively control the release of ABE and VES in acidic tumor environment. Notably, the incorporation of HA greatly reduced the release of dual drug under normal tissue environment (pH 7.4), which solves the problem of increased drug release caused by the high powderization of CaP. Moreover, even HA/CaP concentrations as high as 200 μg/mL hardly affected the viability of normal cell; thus, HA/CaP has excellent in vitro biocompatibility. In addition, the presence of the HA layer greatly reduced the release of drugs in normal cell; therefore, making HA/CaP show weaker lethality to normal cell but maintains toxicity to cancer cell. That is why HA/CaP/ABE-VES exhibits a stronger synergistic effect than CaP/ABE-VES. The inorganic/organic composite material has better tumor selectivity and is more suitable for anti-tumor drug delivery. This research established a new drug delivery strategy for breast cancer and provides a new treatment choice (i.e., ABE) for tumor treatment.

Declarations

Credit author statement

Yuanyuan Liu participated in investigating and writing-original draft. Hui Li participated in conceptualization. Qiaomei Sun supervised the study. Na Gan was responsible for methodology. Shuangshuang Zhang participated in data curation. Xin Wei was in charge of formal analysis. Xiuyun Ren and Xi Xiang performed experiments for revision.

Conflicts of interest

There are no conflicts to declare.

Acknowledgment

We appreciate Hui Wang for helping with SEM characterization from the Analytical & Testing Center of Sichuan University.

References

1. Johnston S, Martin M, Di Leo A, et al (2019) MONARCH 3 final PFS: a randomized study of abemaciclib as initial therapy for advanced breast cancer. NPJ breast cancer 5:5. DOI: 10.1038/s41523-018-0097-z.
2. Dickler MN, Tolaney SM, Rugo HS, et al (2017) MONARCH 1, A Phase II Study of Abemaciclib, a CDK4 and CDK6 Inhibitor, as a Single Agent, in Patients with Refractory HR+/HER2- Metastatic

Breast Cancer. Clin Cancer Res 17(23): 5218–5224. DOI: 10.1158/1078-0432.CCR-17-0754.

3. Taniguchi K, Karin M (2018) NF-κB, inflammation, immunity and cancer: coming of age. Nature reviews. Immunology 121:556–571. DOI: 10.1016/j.ijbiomac.2018.10.049.
4. Klein ME, Kovatcheva M, Davis LE, Tap WD, Koff A (2018) CDK4/6 Inhibitors: The Mechanism of Action May Not Be as Simple as Once Thought. Cancer cell 1(34):9–20. DOI: 10.1016/j.ccell.2018.03.023.
5. Jiang Q (2017) Natural Forms of Vitamin E as Effective Agents for Cancer Prevention and Therapy. Adv Nutr 6(8):850–867. DOI: 10.3945/an.117.016329.
6. Hou L, Tian C, Chen D, Yuan Y, Yan Y, Huang Q, Zhang H, Zhang Z (2019) Investigation on vitamin e succinate based intelligent hyaluronic acid micelles for overcoming drug resistance and enhancing anticancer efficacy. Eur J Pharm SCIs 140:105071. Doi:10.1016/j.ejps.2019.105071
7. Huang P, Ao J, Zhou L, Su Y, Huang W, Zhu X, Yan D (2016) Facile Approach To Construct Ternary Cocktail Nanoparticles for Cancer Combination Therapy. Bioconjugate chem 7(27):1564–1568. DOI: 10.1021/acs.bioconjchem.6b00158.
8. Chou T-C (2010) Drug combination studies and their synergy quantification using the Chou-Talalay method. Cancer Res 2(70):440–446. DOI: 10.1158/0008-5472.CAN-09-1947.
9. D'Mello SR, Cruz CN, Chen M-L, Kapoor M, Lee SL, Tyner KM (2017) The evolving landscape of drug products containing nanomaterials in the United States. Nat Nanotechnol 6(12):523–529. DOI: 10.1038/nnano.2017.67.
10. Min Y, Caster JM, Eblan MJ, Wang AZ (2015) Clinical Translation of Nanomedicine. Chem Rev 19(115):11147–11190. DOI: 10.1021/acs.chemrev.5b00116.
11. Raafat, A.I., Kamal, H., Sharada, H.M. et al. (2020) Radiation Synthesis of Magnesium Doped Nano Hydroxyapatite/(Acacia-Gelatin) Scaffold for Bone Tissue Regeneration: In Vitro Drug Release Study. J Inorg Organomet Polym 30, 2890–2906. DOI: 10.1007/s10904-019-01418-3
12. Kaczmarek, M, Jurczyk, K, Koper, J K, Paszel-Jaworska, A, Jurczyk, M U (2016) In vitro biocompatibility of anodized titanium with deposited silver nanodendrites. J Mater Sci 51(11), 5259-5270.DOI: 10.1007/s10853-016-9829-3
13. Huang G, Huang H (2018) Hyaluronic acid-based biopharmaceutical delivery and tumor-targeted drug delivery system. J Control Release 278:122–126. DOI: 10.1016/j.jconrel.2018.04.015.
14. Ravar F, Saadat E, Gholami M, Dehghankelishadi P, Mahdavi M, Azami S, Dorkoosh FA (2016) Hyaluronic acid-coated liposomes for targeted delivery of paclitaxel, in-vitro characterization and in-vivo evaluation. J Control Release 229:10–22. DOI: 10.1016/j.jconrel.2016.03.012.
15. Xiong H, Du S, Ni J, Zhou J, Yao J (2016) Mitochondria and nuclei dual-targeted heterogeneous hydroxyapatite nanoparticles for enhancing therapeutic efficacy of doxorubicin. Biomaterials 94: 70–83. DOI: 10.1016/j.biomaterials.2016.04.004.
16. Lee MS, Lee JE, Byun E, Kim NW, Lee K, Lee H, Sim SJ, Lee DS, Jeong JH (2014) Target-specific delivery of siRNA by stabilized calcium phosphate nanoparticles using dopa-hyaluronic acid conjugate. J Control Release 192:122–130. DOI: 10.1016/j.jconrel.2014.06.049.

17. Ridi F, Meazzini I, Castroflorio B, Bonini M, Berti D, Baglioni P (2017) Functional calcium phosphate composites in nanomedicine. Adv Colloid Interfac 244:281–295. DOI: 10.1016/j.cis.2016.03.006.
18. Qi C, Lin J, Fu L-H, Huang P (2018) Calcium-based biomaterials for diagnosis, treatment, and theranostics. Chem Soc Rev 2(47): 357–403. DOI: 10.1039/c6cs00746e.
19. Lin K, Wu C, Chang J (2014) Advances in synthesis of calcium phosphate crystals with controlled size and shape. Acta Biomater 10(10):4071–4102. DOI: 10.1016/j.actbio.2014.06.017.
20. Guo X, Yan H, Zhao S, Li Z, Li Y, Liang X (2013) Effect of calcining temperature on particle size of hydroxyapatite synthesized by solid-state reaction at room temperature. Adv Powder Techno 6(24):1034–1038. DOI: 10.1016/j.apt.2013.03.002.
21. Kapri S, Maiti S, Bhattacharyya S (2016) Lemon grass derived porous carbon nanospheres functionalized for controlled and targeted drug delivery. Carbon 100:223–235. DOI: 10.1016/j.carbon.2016.01.017.
22. Bastakoti B-P, Inuoe M, Yusa S-i, Liao S-H, Wu KC-W, Nakashima K, Yamauchi Y (2012) A block copolymer micelle template for synthesis of hollow calcium phosphate nanospheres with excellent biocompatibility. Chem Commun 52(48):6532–6534. DOI: 10.1039/c2cc32279j.
23. Liu T-Y, Chen S-Y, Liu D-M, Liou S-C (2005) On the study of BSA-loaded calcium-deficient hydroxyapatite nano-carriers for controlled drug delivery. J Control Release 1(107):112–121. DOI: 10.1016/j.jconrel.2005.05.025.
24. Matsumoto T, Okazaki M, Inoue M, Yamaguchi S, Kusunose T, Toyonaga T, Hamada Y, Takahashi J (2004) Hydroxyapatite particles as a controlled release carrier of protein. Biomaterials 17(25): 3807–3812. DOI: 10.1016/j.biomaterials.2003.10.081.
25. Oonishi H, Hench LL, Wilson J, Sugihara F, Tsuji E, Kushitani S, Iwaki H (1999) Comparative bone growth behavior in granules of bioceramic materials of various sizes. J. Biomed Mater Res 1(44):31–43. DOI: 10.1002/(sici)1097-4636(199901)44:1<31::aid-jbm4>3.0.co;2-9.
26. Xie Y, Liu Y, Wang Y, Wang S, Jiang T (2012) Chitosan matrix with three dimensionally ordered macroporous structure for nimodipine release. Carbohyd Polym 4(90):1648–1655. DOI: 10.1016/j.carbpol.2012.07.045.
27. Li W-M, Chen S-Y, Liu D-M (2013) In situ doxorubicin-CaP shell formation on amphiphilic gelatin-iron oxide core as a multifunctional drug delivery system with improved cytocompatibility, pH-responsive drug release and MR imaging. Acta biomaterialia. 2(9):5360–5368. DOI: 10.1016/j.actbio.2012.09.023.
28. Ding G-J, Zhu Y-J, Qi C, Lu B-Q, Chen F, Wu J (2015) Porous hollow microspheres of amorphous calcium phosphate: soybean lecithin templated microwave-assisted hydrothermal synthesis and application in drug delivery. J Mater Chem B 9(3):1823–1830. DOI: 10.1039/c4tb01862a.
29. Han S-Y, Han HS, Lee SC, Kang YM, Kim I-S, Park JH (2011) Mineralized hyaluronic acid nanoparticles as a robust drug carrier. J Mater Chem 22(21):7996. DOI: 10.1039/c1jm10466g.
30. Zhu, Wei Bo; Chen, Jia; Yan, Tin Ting; Chen, Qing Hua (2013) Effect of Konjac Glucomannan Content on the Structure and Properties of Sodium Hyaluronate/Chitosan/Konjac Glucomannan Composite

Films. AMR 738:67–72. DOI: 10.4028/www.scientific.net/AMR.738.67.

31. Liang Y-H, Liu C-H, Liao S-H, Lin Y-Y, Tang H-W, Liu S-Y, Lai I-R, Wu KC-W (2012) Cosynthesis of cargo-loaded hydroxyapatite/alginate core-shell nanoparticles (HAP@Alg) as pH-responsive nanovehicles by a pre-gel method. ACS Appl Mater Inter 12(4): 6720–6727. DOI: 10.1021/am301895u.
32. Orrenius S, Zhivotovsky B, Nicotera P (2003) Regulation of cell death: the calcium-apoptosis link. Nat Rev 7(4):552–565. DOI: 10.1038/nrm1150.
33. Zingg J-M, Azzi A, Meydani M (2017) α-Tocopheryl Phosphate Induces VEGF Expression via CD36/PI3Kγ in THP-1 Monocytes. J Cell Biochem 7(118):1855–1867. DOI: 10.1002/jcb.25871.
34. Chou T-C (2006) Theoretical basis, experimental design, and computerized simulation of synergism and antagonism in drug combination studies. Pharmacol Rev 3(58): 621–681. DOI: 10.1124/pr.58.3.10.
35. Qiu C, Wei W, Sun J, Zhang H-T, Ding J-S, Wang J-C, Zhang Q (2016) Systemic delivery of siRNA by hyaluronan-functionalized calcium phosphate nanoparticles for tumor-targeted therapy. Nanoscale 26(8):13033–13044. DOI: 10.1039/c6nr04034a.

Figures

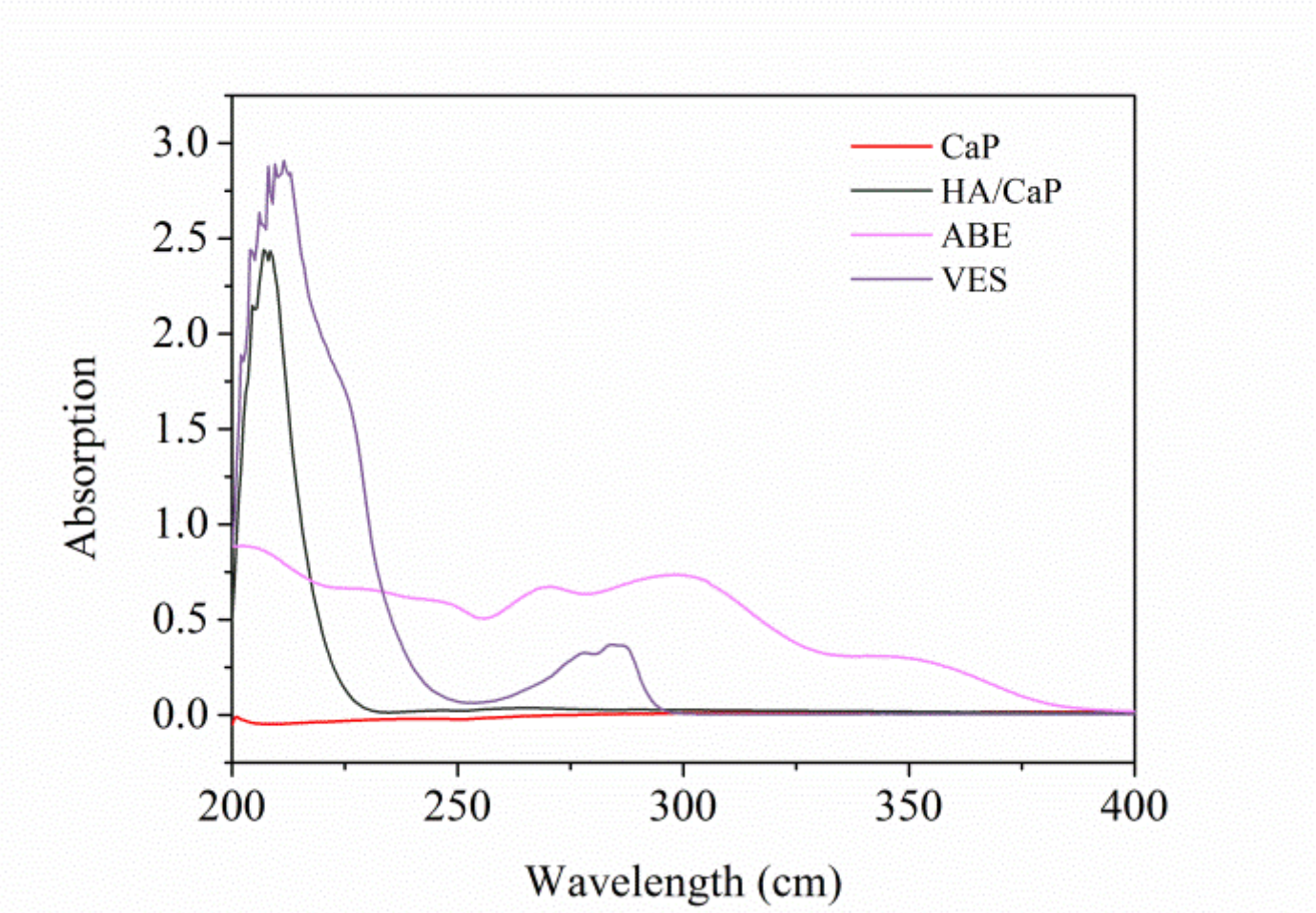

Figure 1

Ultraviolet spectra of ABE, VES, CaP and HA/CaP

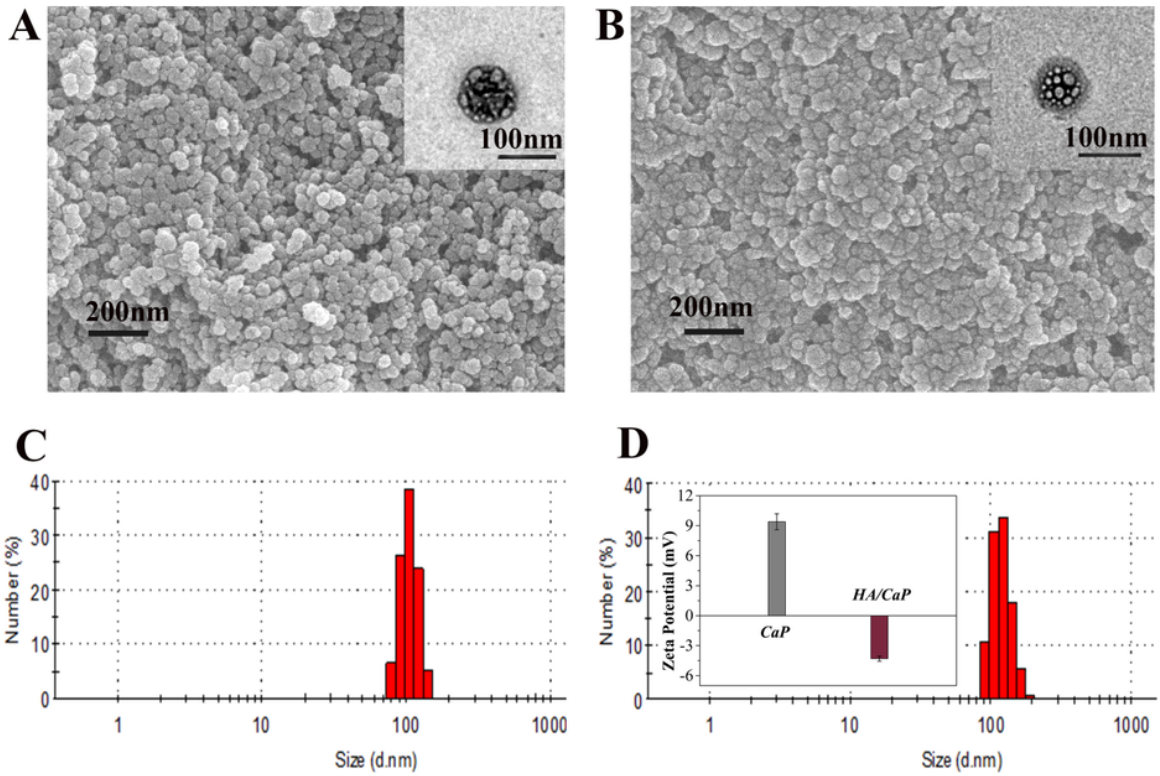

Figure 2

SEM image and TEM partial magnification of CaP (A) and HA/CaP (B); DLS particle size distribution of CaP (C) and HA/CaP (D); Zeta potential diagram (D)

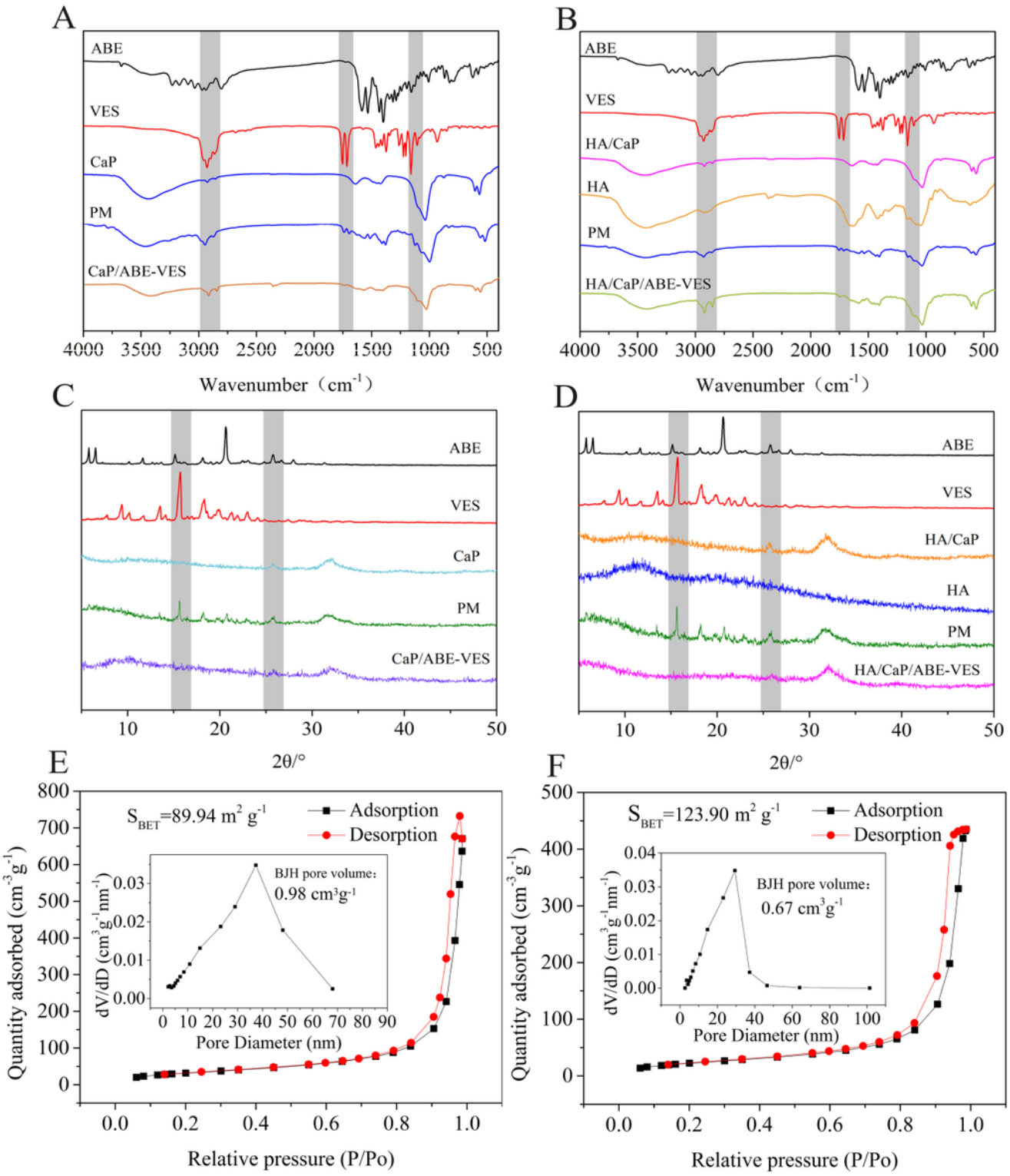

Figure 3

Infrared spectra (A, B); XRD patterns (C, D); N2 adsorption-desorption isotherm and BJH desorption pore size distribution curve of CaP (E) and HA/CaP (F)

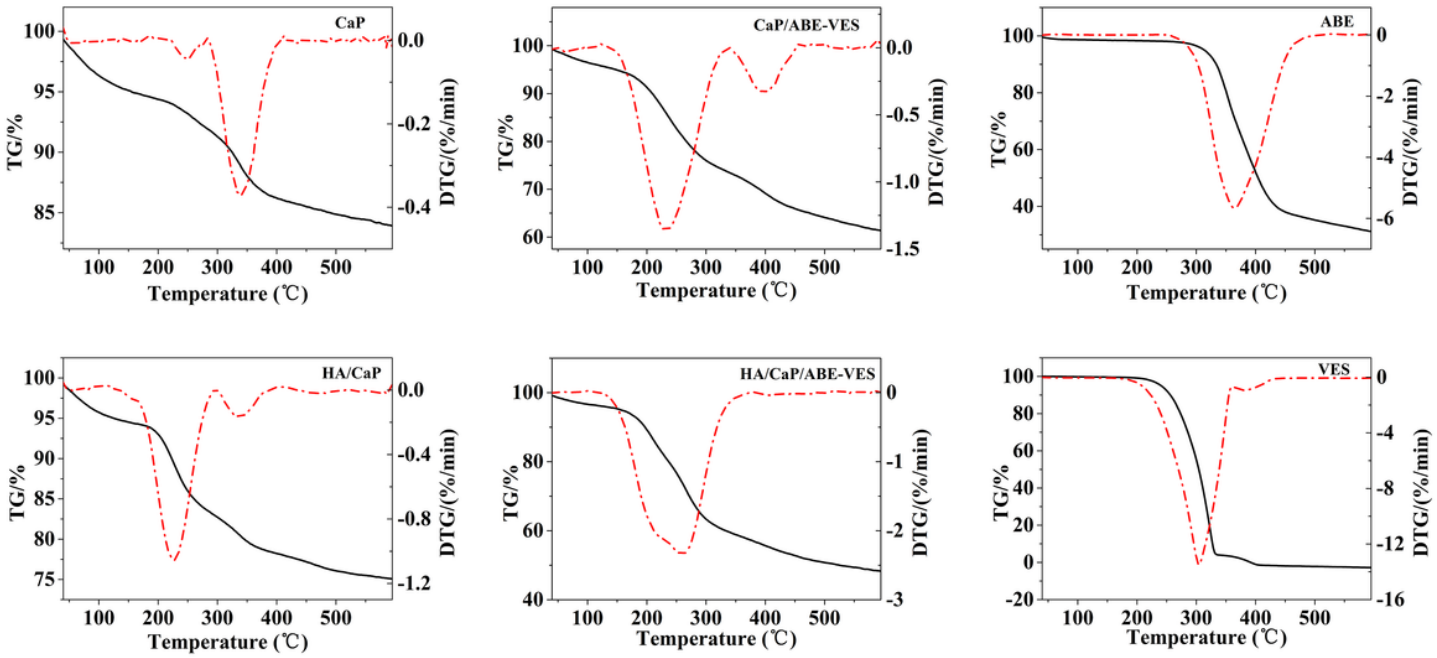

Figure 4

TG curves of single drug; blank and drug-loaded materials

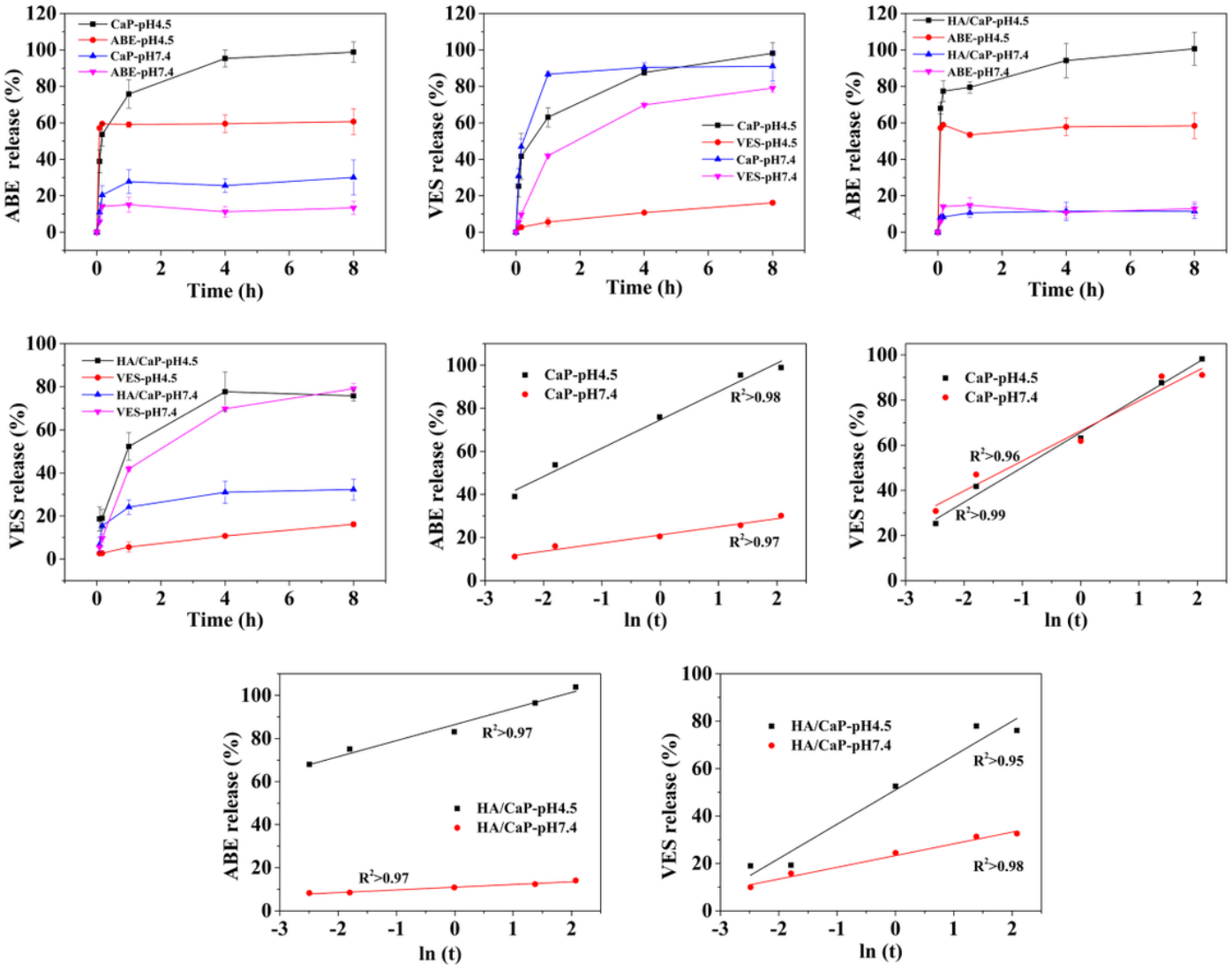

Figure 5

In vitro drug release curves; cumulative release percentage versus natural logarithm of time plot for drug-loaded system

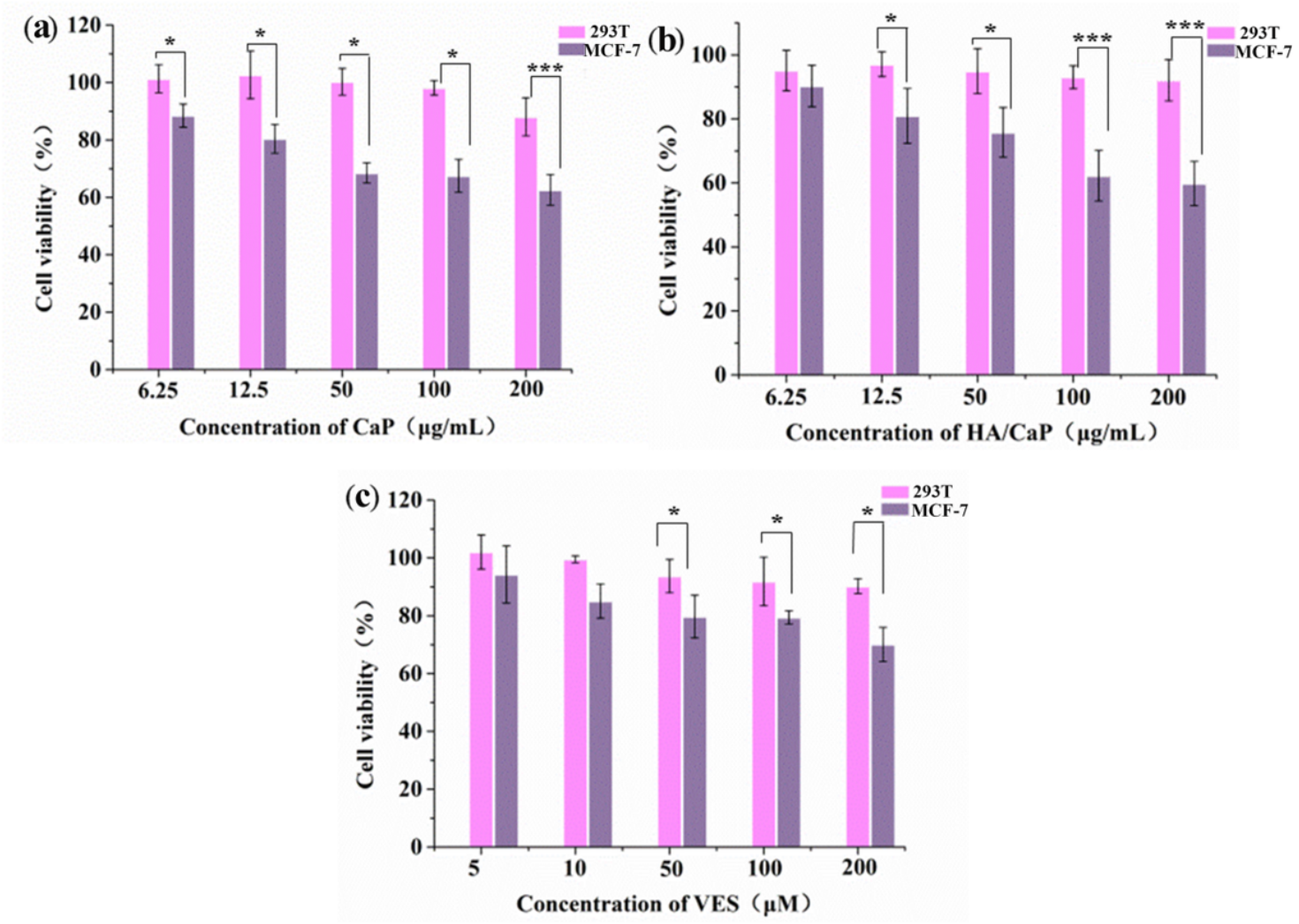

Figure 6

Cytotoxicity of CaP (a) HA/CaP (b) and VES (c)

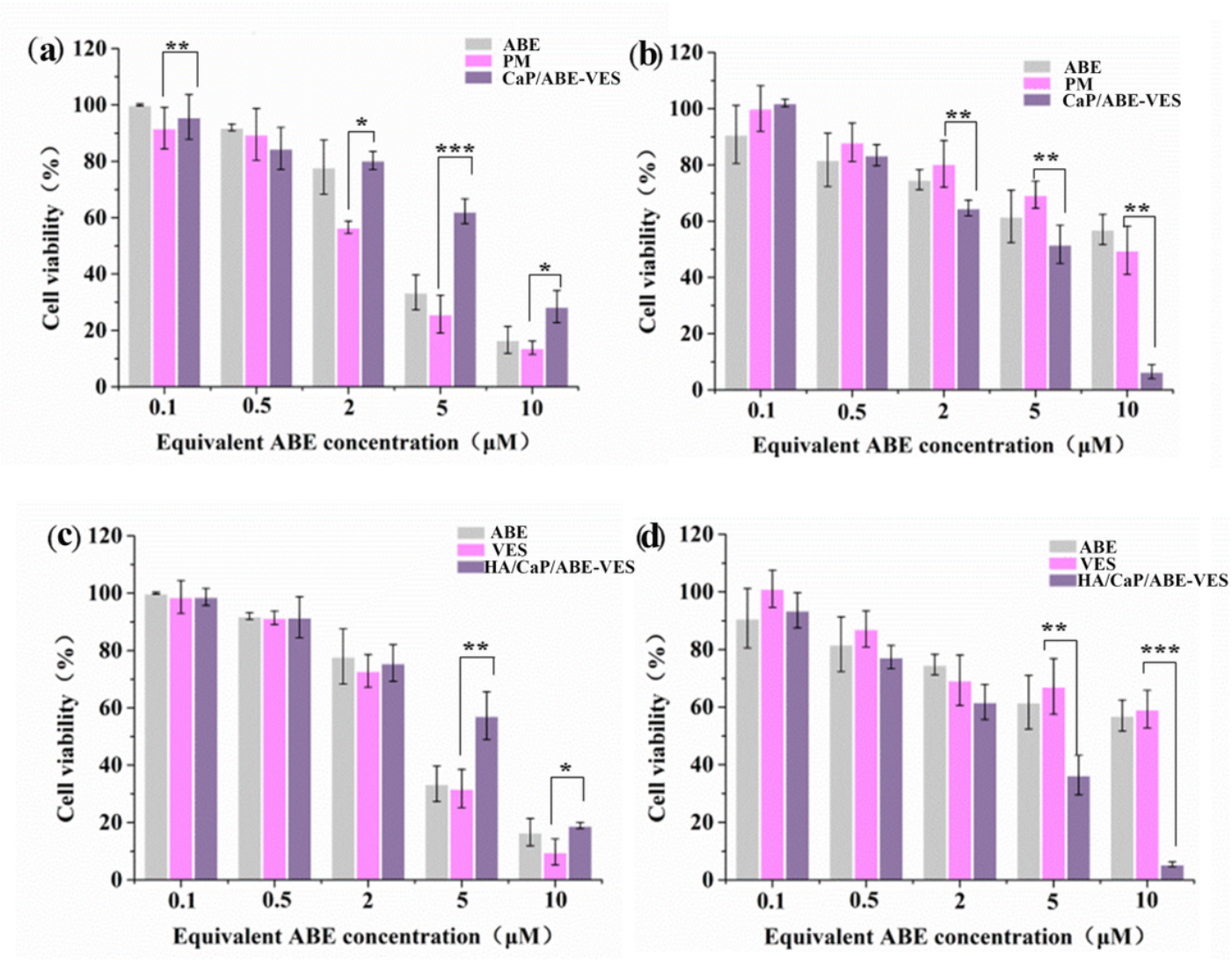

Figure 7

Cell viability of CaP/ABE-VES, HA/CaP/ABE-VES, PM in 293T cells (a, c), and MCF-7 cells(b, d)

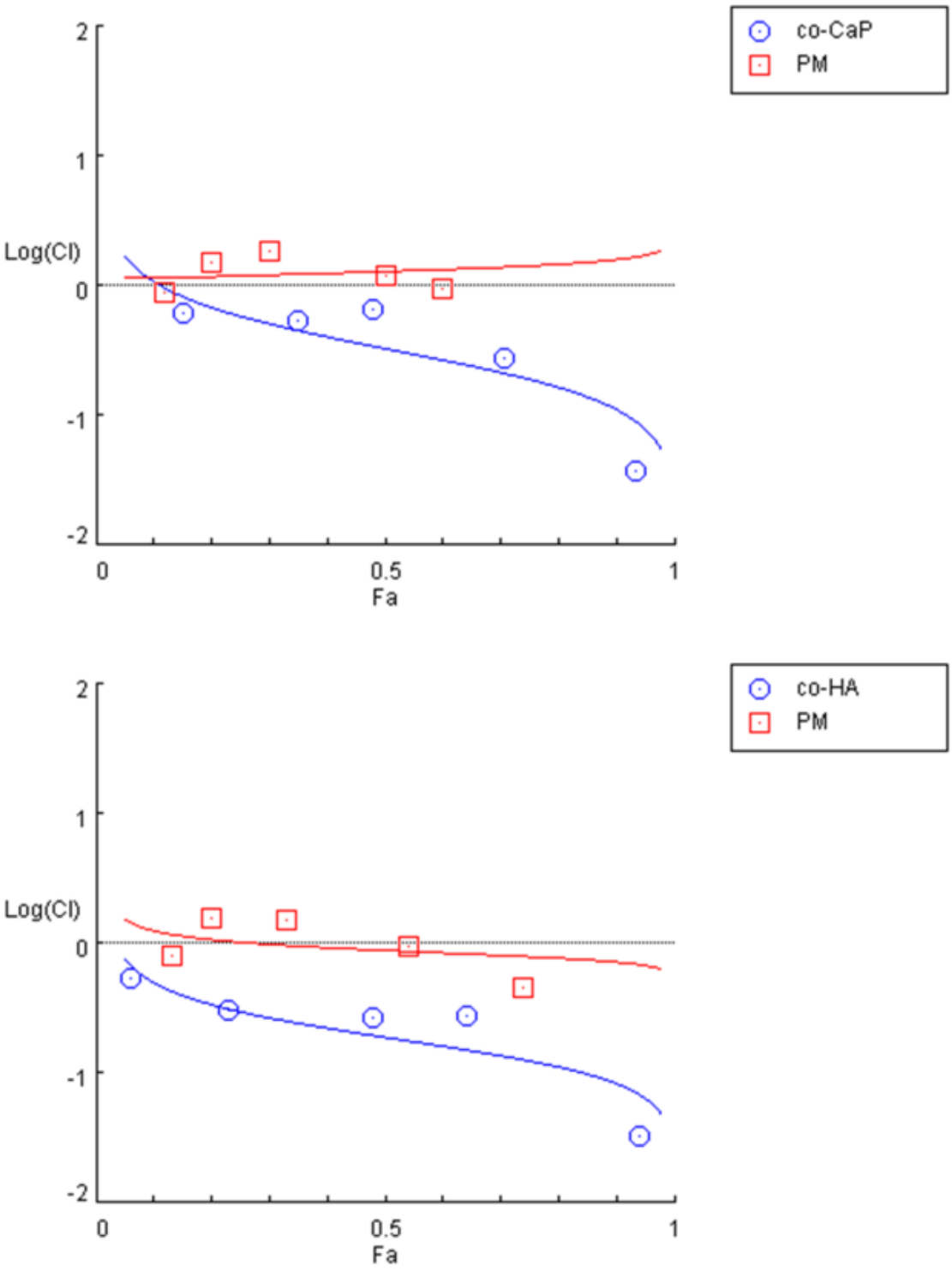

Figure 8

Fa-Log (CI) Plot of CaP/ABE-VES(co-CaP) and HA/CaP/ABE-VES(co-HA)

Supplementary Files

This is a list of supplementary files associated with this preprint. Click to download.

- Supplementarymaterial.docx